Electronic Supplementary Material (ESI) for Nanoscale Horizons.

Supplementary Information: Ferroelectric Polymer-based Artificial Synapse for Neuromorphic Computing

*Sungjun Kim,[‡a,b] Keun Heo,[‡b] Sunghun Lee,[b] Seunghwan Seo,[b] Hyeongjun Kim,[b] Jeongick Cho,[b] Hyunkyu Lee,[b] Kyeong-Bae Lee,[b] and Jin-Hong Park [*b]*

[a] *Foundry Division, Samsung Electronics Co. Ltd., Youngin 17113, Korea*
[b] *Department of Electrical and Computer Engineering, Sungkyunkwan University, Suwon 16419, Korea*

† These authors contributed equally to this work.
* Corresponding author's email address: jhpark9@skku.edu (J.-H. P)

Decay characteristics of EPSC and IPSC

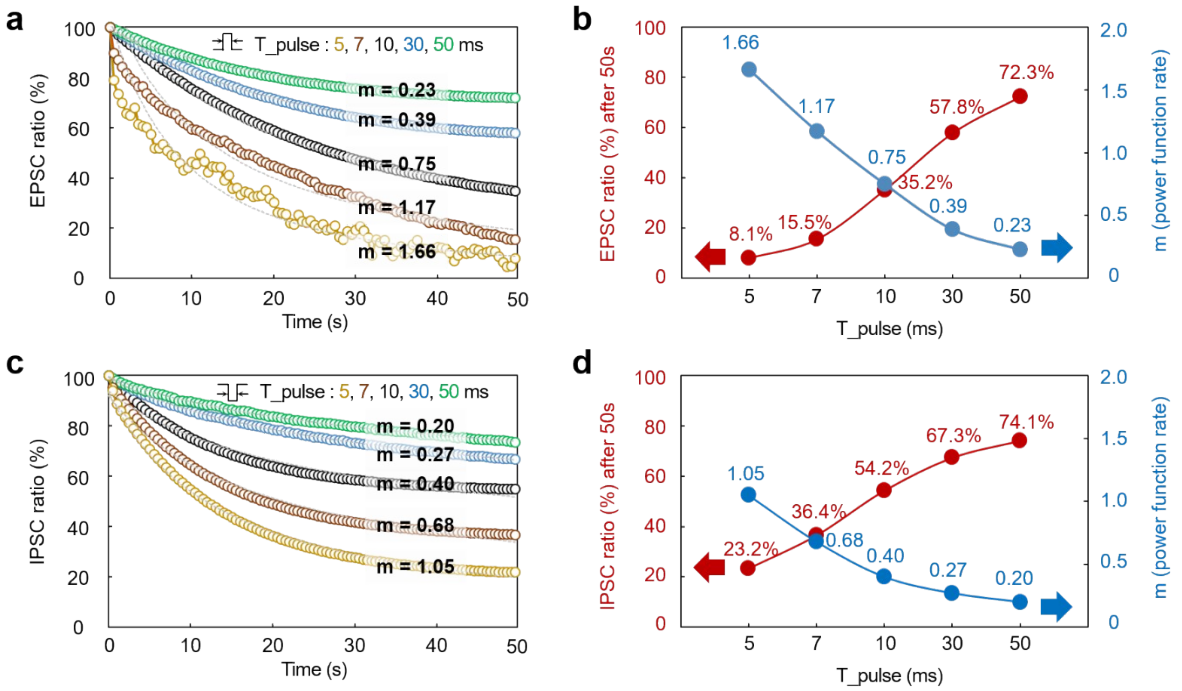

Fig. S1. Decay characteristics of EPSC (amplitude of 5 V) and IPSC (amplitude of −5 V): (a) EPSC ratio (EPSC at a certain time/EPSC at t = 0 s) as a function of time with respect to pulse width. (b) EPSC ratio and power function rate (m) extracted from the EPSC curves, which are plotted as a function of pulse width. (c) IPSC ratio (IPSC at a certain time/IPSC at t = 0 s) as a function of time with respect to pulse width. (d) IPSC ratio and power function rate (m) extracted from the IPSC curves, which are plotted as a function of pulse width.

The EPSC and IPSC ratios were investigated with respect to various pulse widths. In the measurement, because the applied spike voltage with an amplitude of 5 V is smaller than the coercive voltage, fully switched domains that generate remnant polarization and less switched domains that cannot retain their switched states exist together. Here, the less switched domains recover to their original states owing to the E-field induced by the neighboring domains, leading to the decay characteristics in EPSC and IPSC. The conductance decay phenomenon over time is analogous to the forgetting phenomenon in neuroscience, which is dependent on the rate of power function (m).[1] As the pulse width increased, the PSC ratios increased, and m-values decreased for both EPSC and IPSC."

Weight updating energy with respect to the pulse amplitude and duration

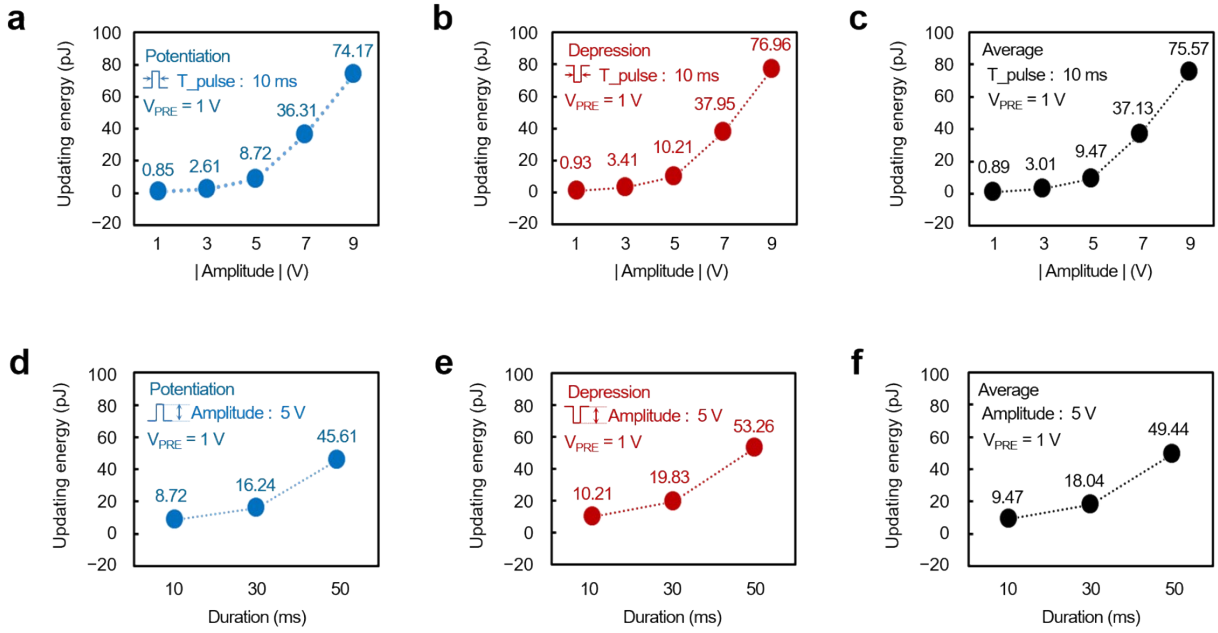

Fig. S2. Weight updating energy with respect to the amplitude of pulses for (a) potentiation and (b) depression. (c) Average updating energy as a function of the pulse amplitude. Weight updating energy with respect to the duration of pulses for (a) potentiation and (b) depression. (c) Average updating energy as a function of the pulse duration.

We investigated the updating energy for the potentiation and depression with respect to the amplitude and duration of spike pulses. The updating energy of FeFET synaptic device can be estimated using the following equation: [2]

$$P_{updating} = V_{spike} \times T_{duration} \times I_{leakage}$$

Here, V_{spike}, T_{duration}, and I_{leakage} denote the amplitude, the duration of the spike, and the gate leakage current flowing across the ferroelectric layer, respectively.

Polarization-voltage hysteresis loops for P(VDF-TrFE) films annealed at four different temperatures

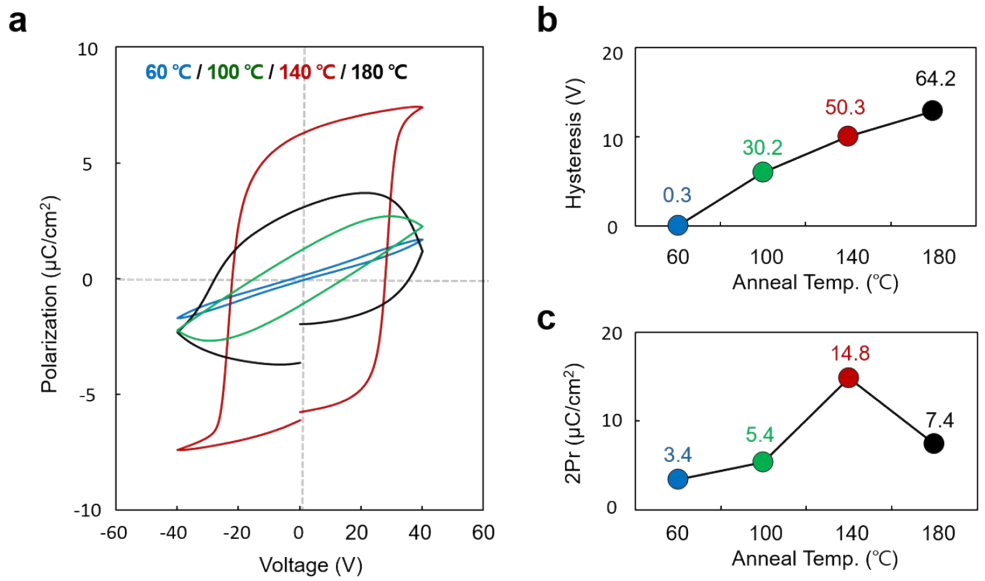

Fig. S3(a) Polarization-voltage hysteresis loops for the P(VDF-TrFE) films annealed at four different temperatures. (b) Hysteresis and (c) remnant polarization (2Pr) with respect to annealing temperatures.

Polarization-voltage hysteresis loops for the P(VDF-TrFE) films were investigated with respect to the annealing temperatures (60, 100, 140, and 180 °C). The metal-ferroelectric-metal (MFM) structures (area: 1 mm^2) were prepared, where 150-nm-thick Pt, 50-nm-thick Au, and 395-nm-thick P(VDF/TrFE) films were used as the bottom electrode, top electrode, and ferroelectric material, respectively. The *P–V* hysteresis was measured at a frequency of 10 Hz. As the annealing temperature increased, the hysteresis window increased (Figs. S3(a),(b)), which is consistent with the result shown in Fig. 2(b) (upper panel). Additionally, the remnant polarization (2Pr) changes with respect to the annealing temperatures in Fig. S3(c) are consistent with the C–V data result shown in Fig. 2(b) (lower panel).

DSC analysis of P(VDF-TrFE) (80/20) copolymer film

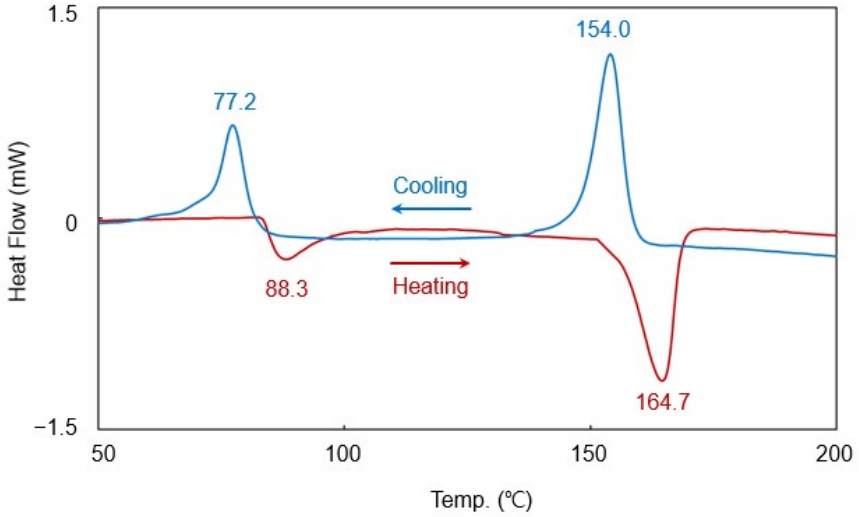

Fig. S4. DSC analysis of P(VDF-TrFE) (80/20) copolymer film.

The differential scanning calorimetry (DSC) analysis for P(VDF-TrFE) (80/20) copolymer film was conducted to find the Curie (T_C: 88.3 ℃) and melting temperatures (T_M: 164.7 ℃). The 1.9 mg of the P(VDF-TrFE) sample was heated from room temperature to 200 ℃ and cooled back to room temperature at a rate of 10 ℃/min. In the heating process, two endothermic peaks were observed at temperatures of 88.3 ℃ and 164.7 ℃. The first peak at a lower temperature corresponds to the T_C, where ferroelectric phase transits to paraelectric phase. The second peak at a higher temperature corresponds to T_M, where polymer chains begin to decompose. Since the P(VDF-TrFE) film is well crystallized to have β-phase domains when annealed between T_C and T_M,[3] the optimal annealing temperature range was determined to be 88.3 – 164.7 ℃.

I_D V_G characteristics of P(VDF-TrFE) FeFET

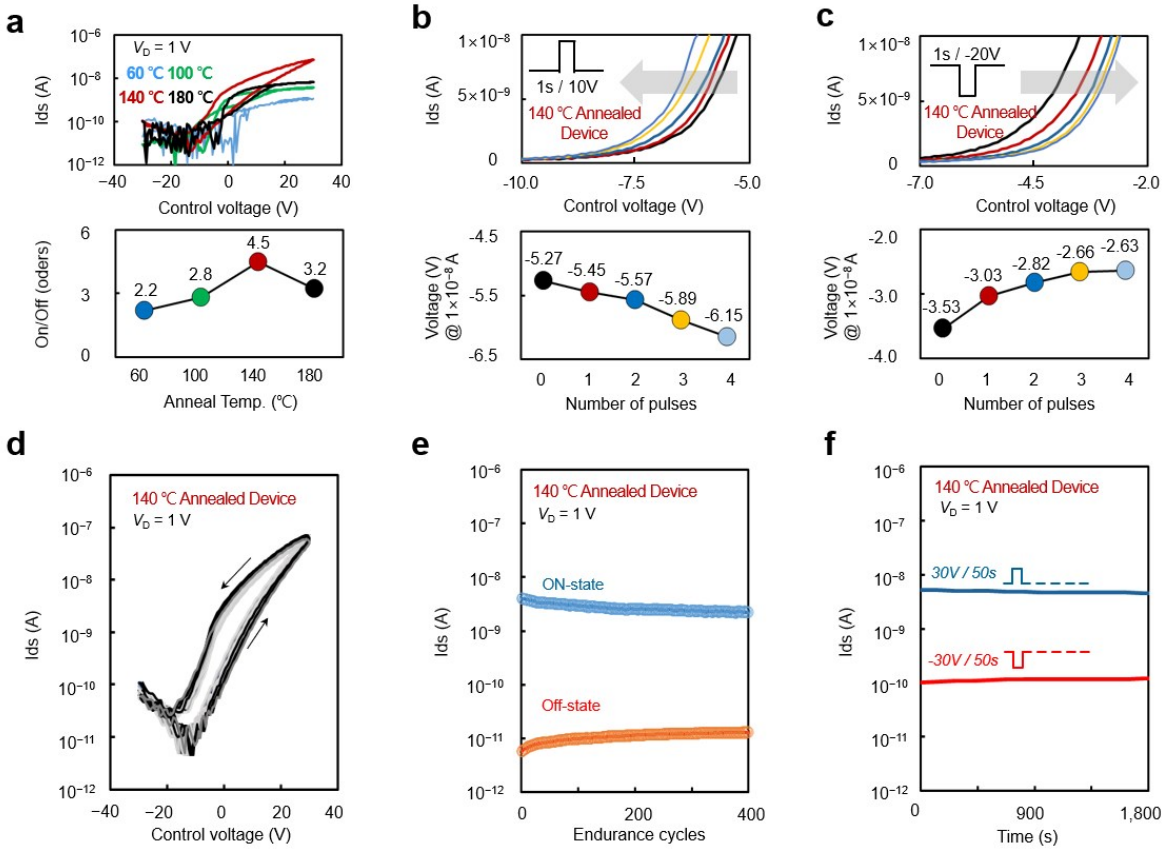

Fig. S5. (a) I_D V_G characteristics of the P(VDF-TrFE) FeFET synapse samples annealed at four different temperatures. I_D V_G characteristic curves in linear scale after applying (b) positive pulses (10V, 1s) and (c) negative pulses (–20V, 1s). (d) 400-times-repeated I_D V_G cyclic curves of the 140 ℃ annealed FeFET. (e) On- and Off-state currents extracted from (d). (f) Retention characteristics of both On- and Off-states up to 1,800 s with the duration of 50 s.

As shown in Fig. S5a, the on/off ratio of the FeFET device was 2.2–4.5. In Fig. S5b and c, we confirmed the left- and right-shifts of the I_D V_G curve as applying consecutively positive and negative pulses, respectively. In addition, to investigate the endurance characteristics of the FeFET, the cyclic measurement of I_D V_G was performed 400 times, as shown in Fig. S5d. Here, On- and Off-states indicate the I_D values at V_G = 0 V when V_G is swept in the negative and positive directions, respectively. On/Off-state ratio was maintained over 2 orders even after 400 cyclic sweeps (Fig. S5e) and the polarized states were confirmed to be maintained well for 1,800 s (Fig. S5f).

Nonlinearity analysis of LTP/LTD curves

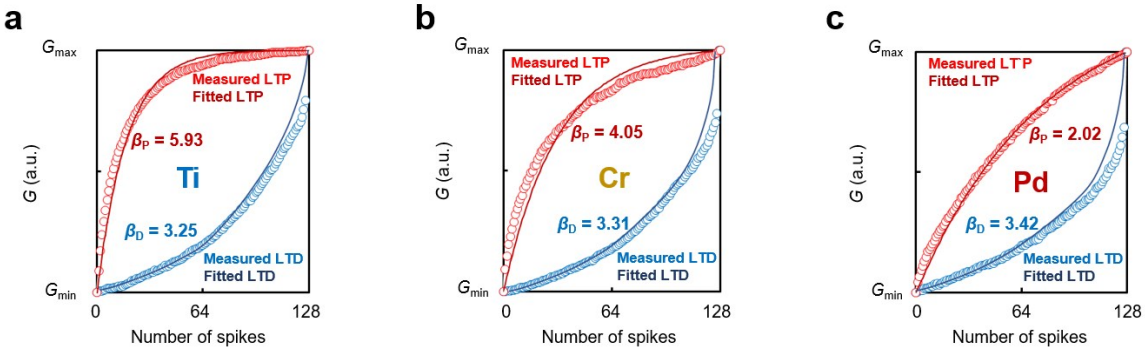

Fig. S6. Nonlinearity (NL) analysis. NL extraction from the LTP/D curves for (a) Ti-, (b) Cr-, and (c) Pd-contacted devices.

The NL value of the LTP/D curve was calculated using the following equations:

$$G_{LTP} = B \cdot (1 - \exp(-P/A_P)) + G_{min}, \quad (1)$$

$$G_{LTD} = -B \cdot (1 - \exp((P - P_{max})/A_D)) + G_{max}, \quad (2)$$

$$B = (G_{max} - G_{min})/(1 - \exp(-P_{max}/A_{P,D})) \quad (3)$$

where G_{LTP} and G_{LTD} are the conductance values of the LTP and LTD regions, respectively. P is the number of applied pulses. A is a parameter representing *NL*. B is a fitting constant used to normalize the conductance range. The A value was extracted from the experimental data using the MATLAB code provided as an open source, and the corresponding *NL* values were derived from tables provided by the same source.[4]

Effective conductance-state ratio

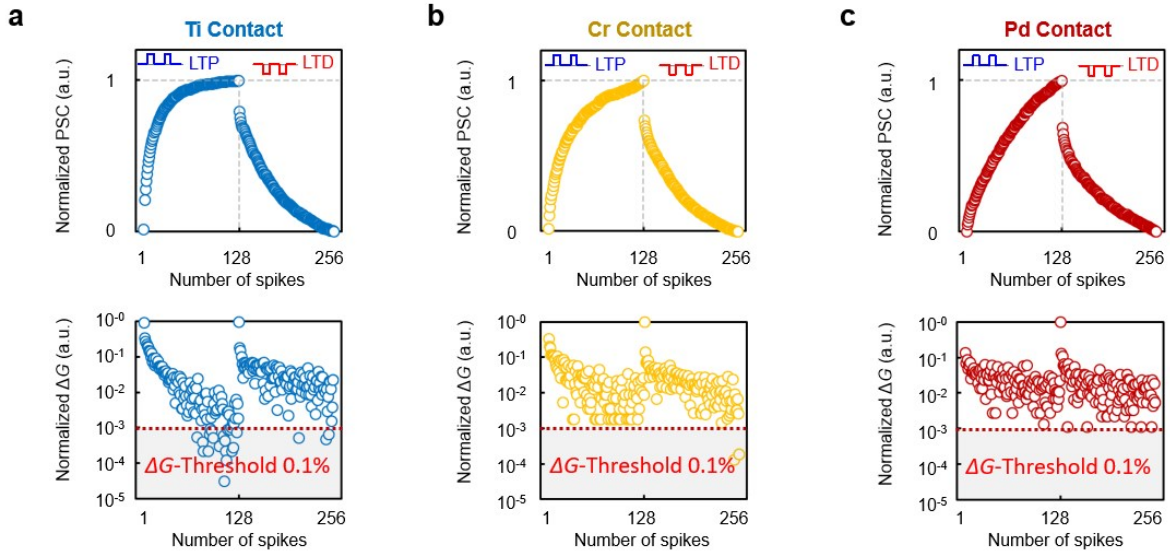

Fig. S7. Normalized PSC and Δ*G* curves as a function of the number of spikes to calculate the effective conductance-state ratio for (a) Ti-, (b) Cr-, and (c) Pd-contacted devices.

The effective conductance-state ratio was defined as the ratio of the number of conductance states in which Δ*G* exceeded a certain percentage of G_{max}/G_{min} (Δ*G*-Threshold) to the total number of conductance states. When a Δ*G*-Threshold is 0.1%, the number of effective conductance-states were 194 (75.8%), 206 (80.5%), and 233 (91.0%) out of total 256 states for Ti-, Cr-, Pd-contacted devices, respectively.

Symmetricity analysis of the LTP/D curves

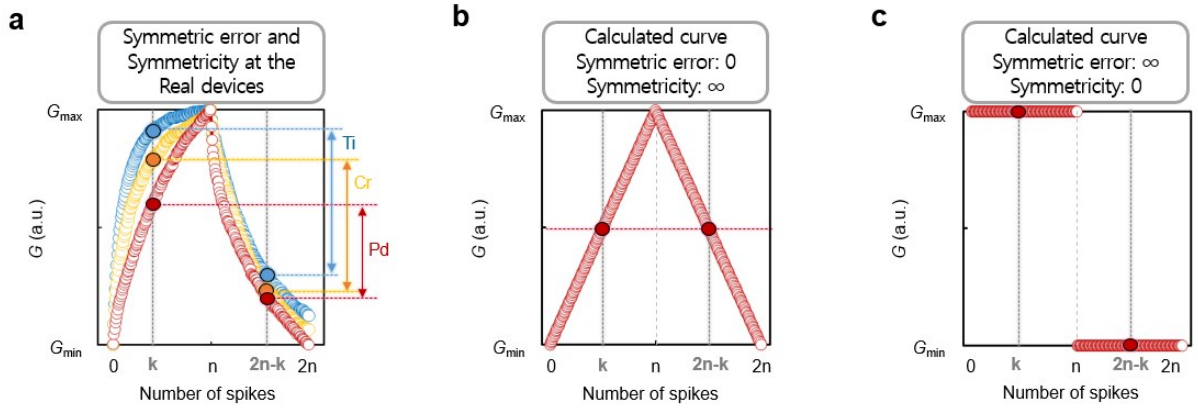

Fig. S8. Symmetricity analysis of the LTP/D curves. (a) LTP/D curves with 2n conductance states for Ti-, Cr-, Pd-contacted devices, where the k^{th} and $(2n-k)^{th}$ conductance states are highlighted. (b) Ideal LTP/D curve with perfect symmetricity and no symmetric error. (c) Worst LTP/D curve with no symmetricity and infinite symmetric error.

Fig. S8a shows the LTP/D curves for the Ti-, Cr-, Pd-contacted devices, and their k^{th} and $(2n-k)^{th}$ conductance states. We defined the symmetricity as the reciprocal of the symmetric error ($\text{symmetricity} = \frac{1}{symmetric\ error}$). Here, the symmetric error was defined as following equation:

$$\text{Symmetric error} = \sum_{k=1}^{k=n} \frac{(G_N(k) - G_N(2n-k))^2}{n} = \sum_{k=1}^{k=n} \frac{((G(k) - G_{min}) - (G(2n-k) - G_{min}))^2}{n(G_{max} - G_{min})^2}$$

$$= \sum_{k=1}^{k=n} \frac{(G(k) - G(2n-k))^2}{n(G_{max} - G_{min})^2}, \text{ where } G_N(k) = \frac{G(k) - G_{min}}{G_{max} - G_{min}}.$$

Here, G_N, G_{MAX}, and G_{MIN} denote the normalized value of conductance, the maximum value of conductance, and the minimum value of conductance. Fig. S8b shows the calculated LTP/D curve with the perfect symmetricity and no symmetric error. Fig. S8c presents the calculated LTP/D curve with no symmetricity and infinite symmetric error.

Estimated recognition rates as a function of epochs

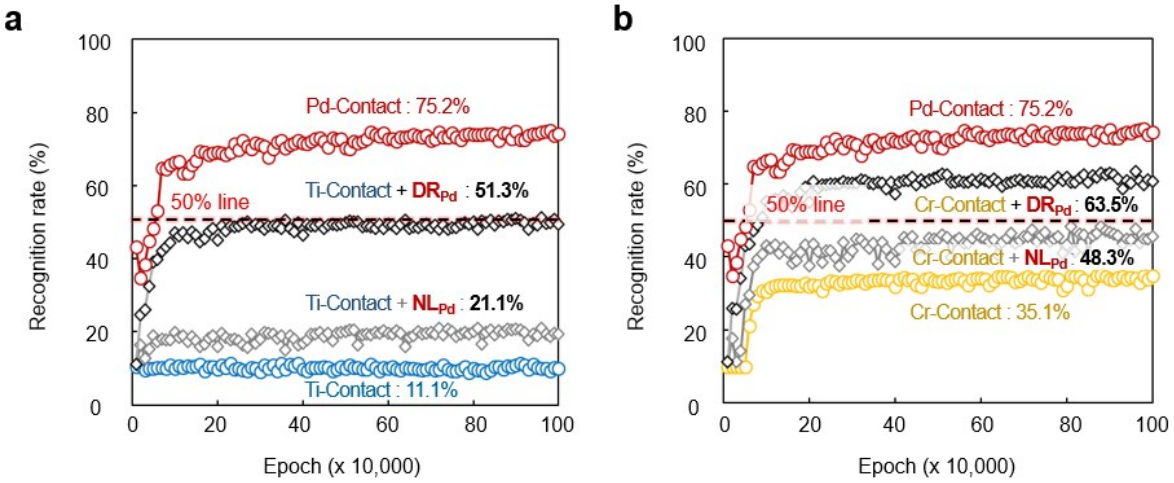

Fig. S9. Estimated recognition rates as a function of epochs, applying NL or DR value of the Pd-contacted device to the (a) Ti- and (b) Cr-contacted devices.

Table S1. Comparison of the maximum recognition rates between reference devices and estimated devices.

Device condition	DR	NL_{LTP}	NL_{LTD}	Max. Recognition rate (%)
Ti-contacted device	2.15	5.39	3.25	11.1
Cr-contacted device	4.86	4.05	3.31	35.1
Pd-contacted device	8.97	2.02	3.42	75.2
Ti-contacted device + NL_{Pd}	2.15	2.02	3.42	21.1
Ti-contacted device + DR_{Pd}	8.97	5.39	3.25	51.3
Cr-contacted device + NL_{Pd}	4.86	2.02	3.42	48.3
Cr-contacted device + DR_{Pd}	8.97	4.05	3.31	63.5

ML-NN simulation result using MNIST handwritten digits dataset

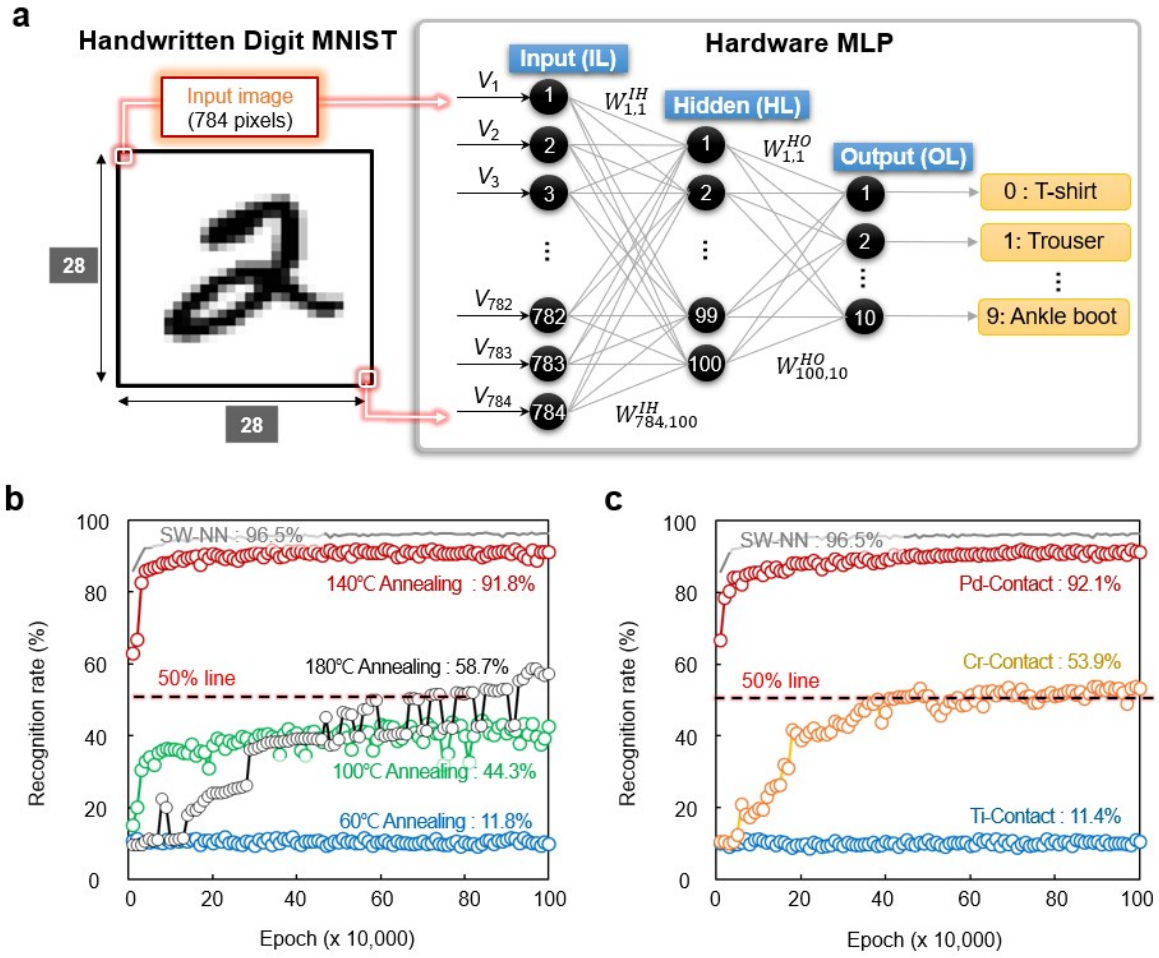

Fig. S10. ML-NN simulation results using MNIST handwritten digits dataset. (a) MNIST handwritten digits dataset (60,000 training images and 10,000 test images) and the ML-NN (one input layer of 784 neurons, one hidden layer of 100 neurons, and one output layer of 10 neurons). The ML-NN simulation results using synaptic parameters obtained from (b) the P(VDF-TrFE) annealing experiment and (c) the contact barrier experiment.

X-SEM images of P(VDF-TrFE) before and after annealing, and T-SEM images w.r.t. annealing temperatures

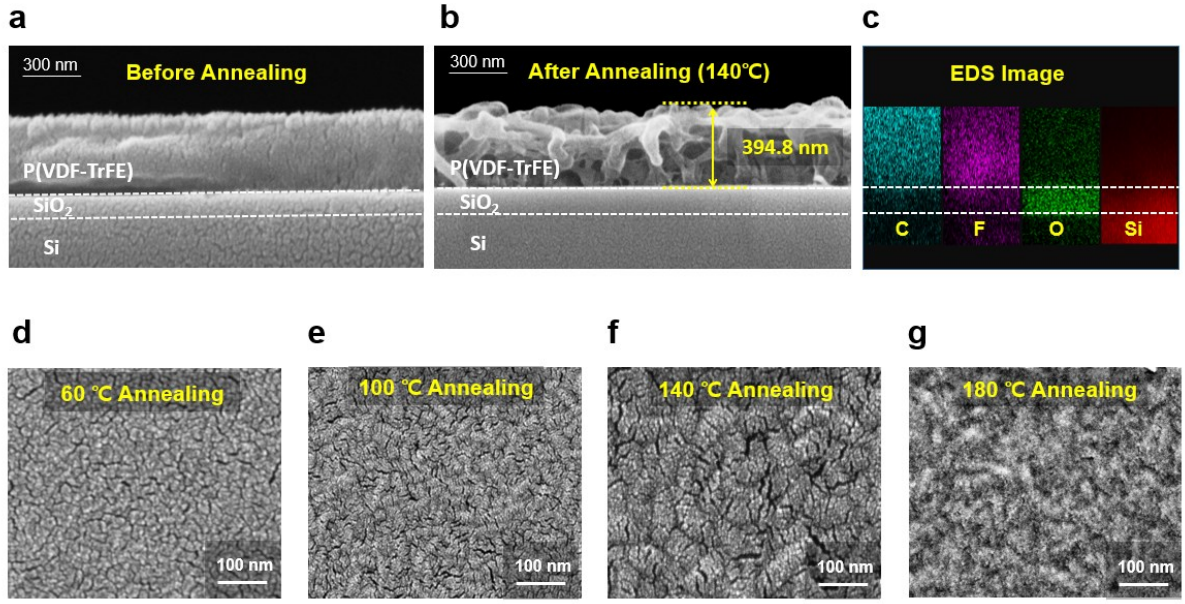

Fig. S11. X-SEM images of P(VDF-TrFE) before and after annealing, and T-SEM images for various annealing temperatures. X-SEM images of the P(VDF-TrFE) film (a) before annealing process and (b) after 140 °C annealing process. (c) EDS mapping image obtained on the cross-section. T-SEM images for (d) 60 °C, (e) 100 °C, (f) 140 °C, and (g) 180 °C annealing processes.

The thickness of P(VDF-TrFE) was confirmed to be 394.8 nm. As shown in the topview scanning electron microscopy (T-SEM) results of Fig. S11d–g, the grain size was maximized after the 140 °C annealing, which is consistent with the AFM analysis in Fig. 2e.

References

1 C. Wan, P. Cai, M. Wang, Y. Qian, W. Huang and X. Chen, *Advanced Materials*, 2020, **32**, 1902434.
2 D. Kuzum, S. Yu, H. P. Wong, *Nanotechnology* 2013, **24**, 382001.
3 D. Mao, M. Quevedo-Lopez, H. Stiegler, B. E. Gnade, H. N. Alshareef, *Organic Electronics* 2010, **11**, 925.
4 Y. Luo, X. Peng, S. Yu, presented at Proceedings of the International Conference on Neuromorphic Systems 2019.